

Efficient Tracking Proposals using 2D-3D Siamese Networks on LIDAR

Jesus Zarzar*, Silvio Giancola*, and Bernard Ghanem

King Abdullah University of Science and Technology (KAUST), Saudi Arabia

{jesusalejandro.zarzartorano,silvio.giancola,bernard.ghanem}@kaust.edu.sa

Abstract

Tracking vehicles in LIDAR point clouds is a challenging task due to the sparsity of the data and the dense search space. The lack of structure in point clouds impedes the use of convolution and correlation filters usually employed in 2D object tracking. In addition, structuring point clouds is cumbersome and implies losing fine-grained information. As a result, generating proposals in 3D space is expensive and inefficient. In this paper, we leverage the dense and structured Bird Eye View (BEV) representation of LIDAR point clouds to efficiently search for objects of interest. We use an efficient Region Proposal Network and generate a small number of object proposals in 3D. Successively, we refine our selection of 3D object candidates by exploiting the similarity capability of a 3D Siamese network. We regularize the latter 3D Siamese network for shape completion to enhance its discrimination capability. Our method attempts to solve both for an efficient search space in the BEV space and a meaningful selection using 3D LIDAR point cloud. We show that the Region Proposal in the BEV outperforms Bayesian methods such as Kalman and Particle Filters in providing proposal by a significant margin and that such candidates are suitable for the 3D Siamese network. By training our method end-to-end, we outperform the previous baseline in vehicle tracking by 12%/18% in Success and Precision when using only 16 candidates.

1. Introduction

Autonomous vehicles have to understand their environment in order to fulfill their driving task. Understanding the road can be achieved by different means: an autonomous agent can either follow the human process, *i.e.* sense the world through RGB images, or rely on more advanced sensors, such as LIDAR devices, which estimate the depth of objects surrounding the agent. On one hand, the process of scene understanding relies on 2D images; on the other hand, it relies on 3D point clouds.

Thanks to the advances in Convolutional Neural Networks (CNNs) [24, 10, 1], algorithms used to process im-

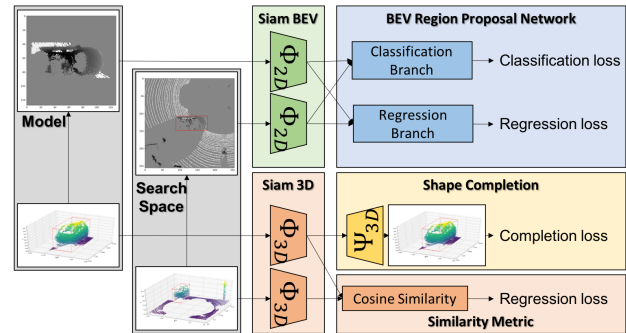


Figure 1. We propose a double Siamese network for both 3D point cloud (orange) and 2D Bird Eye View (green) representation of the LIDAR data to track vehicles in autonomous driving settings. We leverage an efficient search space using a Region Proposal Network (blue) on top of the BEV Siamese network to generate fast proposals. We leverage a shape completion regularization (yellow) on top of the 3D Siamese network for a semantic similarity metric.

ages are on par with human performances in object detection, tracking, and segmentation tasks making the use of RGB images ubiquitous. However, cameras still suffer in low-light conditions and when objects lack texture. These hard conditions could confuse any algorithm the same way they would confuse a human driver. Furthermore, due to our limited passive sensing, slow reaction time, and limited attention capacity, humans are not meant to be drivers. Thus, it is not enough to be on par with humans when it comes to dangerous tasks such as driving.

Understanding the road, the actors involved and their dynamics is an arduous task if relying only on visual information. In order to exceed human performances in driving, it is necessary to introduce super-human sensing. LIDAR sensors are capable of providing more detailed and robust environment information than cameras due to their depth sensing. They estimate depth using the Time-of-Flight principle which is insensitive to texture, and are robust to natural environment light since they operate using active laser scans. Therefore, LIDARs are suitable sensors which can provide reliable space information. However, it is more complex to manipulate and analyze point cloud data generated by LI-

DAR sensors when compared with images due to the extra dimension and sparsity of point clouds.

This work focuses on 3D vehicle tracking, *i.e.* following in real-time a vehicle whose position is known only at an initial frame. Current methods either leverage a voxelization of the space or projections of the points into a frontal view, top view, or a combination of both. However, pre-processing a point cloud with these methods leads to a loss of fine-grained information. Giancola *et al.* [9] introduced the first 3D Siamese Tracker with point cloud input. They show an improvement in tracking by regularizing the Siamese latent space to resemble a shape completion latent space. However, they only solve for a similarity metric between candidates sampled using an exhaustive search guaranteed to contain the ground truth bounding box for each frame. In other words, they disregard the problem of generating proposals which include the ground truth and do not comprehensively analyze the continuous search space.

In this paper, we tackle the problem of efficiently generating proposals for vehicle tracking in LIDAR point clouds. We propose a double Siamese network that encodes both point cloud and 2D Bird Eye View (BEV) information. The search problem is tackled by leveraging an efficient Region Proposal Network (RPN) which relies on the latent representation of 2D BEV images. Proposals generated by the RPN are exploited in the 3D LIDAR point cloud by using a 3D Siamese network regularized for shape completion. An overview of our pipeline is shown in Figure 1. Our 2D Siamese network is based on the SiamRPN [16] object tracker to generate proposals while our 3D Siamese network is based on [9] to provide a similarity measure between candidate vehicles and a model shape from 3D point clouds data. We show that the BEV representation contains enough information to provide good-enough candidates which are successively discarded using the 3D Siamese features for the tracking task.

Contributions: To sum up, our contributions are threefold:

1. We provide an efficient search space using a Region Proposal Network in the Bird Eye View space for the task of Vehicle Tracking in Autonomous Driving settings.
2. We train a double Siamese network end-to-end so to learn proposals and similarity scores simultaneously.
3. We show that using both 2D and 3D Siamese networks and regularizing for shape completion improves performances by 12%/18% in both Success and Precision with respect to the state-of-the-art proposed in [9] when processing fewer candidates.

2. Related Work

Our work takes insights from Generic Object Tracking, Vehicle Detection and Search Strategy in Tracking settings.

2.1. Generic Object Tracking

Generic Object Tracking focuses on following the trajectory of generic *patches* that represent generic objects [20], people [18], vehicles [8] or visual attributes [12]. The problem is commonly tackled through *tracking-by-detection*, where a *model representation* is built after the first frame and a *search space* is constructed weighting computational costs versus denser space sampling. Algorithms generally use visual and shape information provided through images [12], depth maps [18, 27], and/or LIDAR point clouds [8, 22].

Siamese Trackers. While earlier works on tracking were based on Correlation Filtering [2], the current state-of-the-art is set by deep Siamese Trackers. Bertinetto *et al.* [3] were the first to introduce a Siamese network for the task of visual object tracking. Valmadre *et al.* [29] improved upon it by leveraging convolutions between patches and a search space to streamline the process. Li *et al.* [17] included a Region Proposal Network to avoid convolving the whole search space. Zhu *et al.* [35] introduced Hard Negative Mining to focus on more challenging samples during training. More recently, Li *et al.* [15] extended the Siamese network by using ResNet-50 as the backbone [10], which achieved state-of-the-art results in the challenging large-scale TrackingNet dataset [20].

2.2. Tracking Vehicles for Autonomous Driving

For vehicle tracking in road settings, the detection problem is typically reduced to 3 degrees of freedom using the hypothesis that vehicles lean on the 3D plane created by the road. Also, Giancola *et al.* [9] leverage vehicles' rigidity to set a constant scale of the object along the tracklets.

Bird Eye View. Luo *et al.* [19] are using exclusively BEV images to detect, track and predict the pose of vehicles in time and space, using a concatenation of BEV images in time. However, they compare their results on a proprietary dataset making them impossible to compare with.

Multi Views. Chen *et al.* [7] leverage in MV3D a fusion between RGB images along with top and frontal views of LIDAR point clouds to detect vehicles in road settings. Ku *et al.* [14] combined in AVOD the information of both BEV and RGB images to generate 3D proposals in an expensive 3D search grid. In our work, we are using exclusively LIDAR data as a more reliable source of information about the scene in low-light and low-texture conditions.

Point Cloud Siamese Trackers. Giancola *et al.* [9] introduced the first 3D Siamese tracker based solely on point

clouds. They regularized the 3D latent space for shape completion and showed improved results in the similarity metric they exploit for tracking. However, they assume an exhaustive search space that guarantees the ground truth sample is included as one of the candidates and disregard the problem of generating candidates. Due to the continuous 3D space and the inevitable drift that occurs while tracking, a smart search space is necessary. In our work, we propose an efficient search space leveraging a Region Proposal Network on the BEV space to provide a limited set of good object candidates.

2.3. Search Strategies

Search spaces for visual tracking are dense when possible, else rely on Kalman filters, Particle filter or Proposal networks. Since dense search space strategies are not transferable in the continuous 3D space, we relate here on Filtering and Proposal methods.

Particle/Kalman Filterings. Particle Filtering selects a set of particles at and around the target according to a Gaussian distribution centered at the previous states, and selects the following set based on the performance of current particles. Kalman filters are a notable exception of Particle filters which estimates a multivariate distribution for each iteration. Alternatively, it is possible to fit a Mixture of Gaussian based on previous states. Kalman and Particle Filters are widely used in robotics [5] and visual object tracking [25, 31]. They fit a distribution based on observations and update that distribution according to the particles’ observations. Blake *et al.* [4] introduced the importance of sampling in particle filtering, Musso *et al.* [21] proposed a regularization to solve for particle collapse, Zhou *et al.* [33] adjusted the number of particles according to an adaptive noise component, Yang *et al.* [30] introduced a hierarchical particle filter based on a coarse-to-fine pipeline, and Zhang *et al.* [32] adopted a multi-task correlation filter to shepherd particles toward the modes of a target state distribution. Recently, Karkus *et al.* [11] proposed a learnable particle filter network with applications on visual localization. In this work, we compare against the particle filtering employed by Giancola *et al.* [9].

3D Object Proposal. 3D Object Proposals can be interpreted as an alternative to particle filter-based sampling. Shin *et al.* [26] provide a proposal method based on point cloud clustering. Even though the method provides interesting results, they do not compare on elaboration times which are too slow for tracking purposes. Chen *et al.* [6] use stereo images in order to propose candidate Bounding Boxes (BBs). They show impressive improvements on KITTI detection by minimizing an energy function that encodes point cloud density, free space, height priors and height contrast. However they rely on RGB images.

Ren *et al.* [24] proposed a Region Proposal Network

(RPN) for the Fast RCNN object detector. Several works focused on adapting this work for use on 3D data. Song *et al.* [28] proposed Deep Sliding Shapes, an amodal 3D object detection framework for RGB-D frames. They find the main orientation of a scene based on a Manhattan Frame module, coupled with an RPN acting on a TSDF representation of the scene to produce 3D proposal BBs. Chen *et al.* [7] proposed MV3D, an object detection network based on RGB images as well as the top and front views of LIDAR point clouds. They have a 3D proposal network based on RPN coupled with a region-based fusion network. Zhou *et al.* [34] proposed VoxelNet, an end-to-end learning method for point cloud based 3D object detection. They learn features on a voxelization of the space and use a fully-convolutional neural network to output region proposals in 3D.

While these methods provide interesting insights for proposals on different sensors, none of them actually leverage exclusively LIDAR information. We motivate the efficient LIDAR BEV representation for proposals and the meaningful 3D point cloud representation for similarity estimation in tracking settings.

3. Methodology

We propose a double Siamese network that leverages both 2D BEV and 3D point cloud representations of LIDAR data. Searching in BEV images is easier than in point clouds, although prone to error due to the coarse appearance information contained in a 2D BEV representation. However, the BEV representation is suitable for proposal generation as soon as it provides a good recall. The fine-grained details contained in the 3D point cloud representation are afterwards used to select the correct candidate among the proposals and refine the search. An overview of our method is shown in Figure 1 for training and in Figure 2 for inference.

3.1. Tracking

We assume the pose of the tracked object to be given for the first frame in a tracklet consisting of a set of LIDAR point clouds. The object’s pose in the first frame is used to initialize a model shape describing the tracked object. This model shape is updated at the end of each tracking step by concatenating points lying inside the predicted bounding box to the current model shape. A model BEV image is constructed from the model shape. The region around the position of the object in the previous frame is used to generate a search BEV image. Both the model and search BEV images are then processed by an RPN in order to produce C candidates for the object’s pose in the current frame. Finally, a 3D siamese network is used to select the tracked object from among the candidates proposed by the RPN.

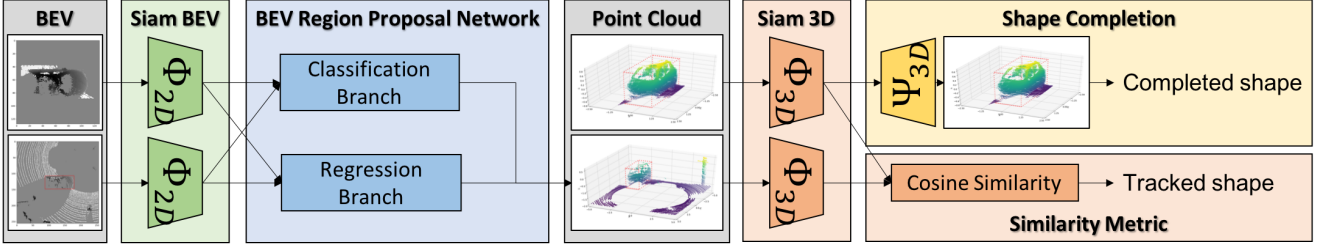


Figure 2. During inference, our model leverages a set of 1445 anchors in the Bird Eye View space. We classify and regress the anchors using a Region Proposal Network to generate a set of C candidates with high recall. Then, the best candidate is selected using the similarity capability of the 3D Siamese network. As a result, we track vehicles using exclusively LIDAR data and reconstruct a more complete vehicle shape.

3.2. Data representation

Bird Eye View Representation. We build our Bird Eye View representation for a given point cloud as an image of size $(N + 2) \times H \times W$ with channels consisting of $N = 1$ vertical slices, the maximum-height map, and the density map. The vertical extent of point cloud data is taken to be $[-1, 1]$ m from the center of the tracked object. A search BEV is generated at each frame by cropping an area of $[5, 5] \times [-5, 5]$ meters around the previously estimated bounding box. An area of $[2.5, 2.5] \times [-2.5, 2.5]$ meters is cropped around the model PC to produce the model BEV image. We generate search and model BEV images of size 255×255 and 127×127 pixels respectively; giving a resolution of approximately 0.04 m per pixel.

Bird Eye View Bounding Boxes. A 3D bounding box projects onto the 2D BEV space as an oriented rectangle. As a consequence, the oriented BEV bounding box is defined by 3 parameters: x , z and α . In vehicle tracking settings there is a bijection between the 2D and 3D bounding boxes since the scale and the height component of the shape are assumed to be constant from the first frame. Also, with the hypothesis of rigid object that characterizes vehicle tracking, the dimension of bounding boxes does not change in time. Note that this hypothesis is respected in the KITTI dataset [8] for the Car, Cyclist and Pedestrian object classes.

3.3. Model Architecture

BEV Siamese Network. We propose a BEV Siamese network that encodes the BEV representation of the model and the search space. The backbone Φ_{2D} is based on AlexNet [13] and pre-trained on ImageNet. We set the number of input channels for the first convolutional layer to be the number of layers that compose our BEV, *i.e.* $N + 2$. We extract a latent feature map of size 6×6 for the model BEV as well as a search space of size 22. Both features maps have a dimension of 256.

BEV Region Proposal Network. We adapt the Region Proposal Network from SiamRPN [16] to generate proposals

for the tracked object. The RPN is composed of a classification branch and a regression branch which convolve separately the model and search space feature maps from the Siamese network and correlate the search space features with the model features. The classification branch selects a set of C candidates from the remaining search space of size $17 \times 17 \times 5$. $K = 5$ different anchors are leveraged to cover multiple angles in the range of $[-5, 5]$ degrees. Note that the classification scores are weighted along a cosine window, as a common practice for 2D object tracking. Successively, the selected anchors are regressed for the x and z coordinates.

Inspired by [24, 19], we regress the position x and z in a different space normalized by the width and length of the tracked object, as defined in Equation (1).

$$\delta_x = \frac{x - x_a}{w}, \quad \delta_z = \frac{z - z_a}{l}, \quad (1)$$

where x_a, z_a are the anchor priors for the pose x and z , and w and l are the width and length of the vehicle which are constant throughout the tracklet.

3D Siamese Network. We use a 3D Siamese network based on [9] to classify the candidate shapes using their 3D point cloud representation. This Siamese network utilizes fine-grained 3D information to classify whether candidate boxes contain the tracked object or not. The backbone of this 3D Siamese network Φ_{3D} consists of 3 PointNet layers [23].

The point cloud representations of proposal shapes are extrapolated in 3D from the parameters of the 2D bounding box. The point cloud representations of our candidate shapes are generated by cropping and centering the 3D point cloud around their corresponding 3D Bounding Box. Also, we enforce point clouds to have 2048 points by either discarding or duplicating points in a uniform random way. The 3D network is trained alongside the RPN to classify candidates generated by the RPN. Note that we regularize our 3D Siamese latent space for shape completion using the feature decoder Ψ_{3D} , as proposed by Giancola *et al.* [9].

3.4. Losses

The BEV Siamese Region Proposal Network is trained to output efficient proposals from the BEV representation, and the 3D Siamese network is trained to select the best proposal by leveraging the candidate’s 3D point cloud representation.

Region Proposal Loss. We train our Region Proposal Network to classify and regress a set of $17 \times 17 \times 5$ anchors along the search space. We adopt a Binary Cross Entropy loss for the classification and a Smooth L1 loss for the regression, as shown in Equation (2).

$$\begin{aligned} \mathcal{L}_{cls} &= \frac{1}{N_t} \sum p_i^* \log(p_i) + (1 - p_i^*) \log(1 - p_i) \\ \mathcal{L}_{reg} &= \frac{1}{2N_p} \sum \gamma_x^i + \gamma_z^i \\ \gamma_x^i &= \begin{cases} 0.5(\delta_x^i - \delta_x^{i*})^2, & \text{if } |\delta_x^i - \delta_x^{i*}| < 1 \\ |\delta_x^i - \delta_x^{i*}| - 0.5, & \text{otherwise} \end{cases} \end{aligned} \quad (2)$$

Where N_t is the total number of samples for a given frame, p_i and p_i^* are the classification score and ground truth label respectively for sample i , N_p is the number of positive samples for a given frame, and δ_x^i and δ_x^{i*} are the regressed and ground truth deltas for sample i . The classification loss is computed across all N_t training samples, and the regression loss is computed using only for the positive samples.

Among the 1445 anchors, we select 48 samples for each frame. From the 48 samples, at most 16 are positive, where positive samples are defined as having an IoU in the range $]0.5, 1]$ with the ground truth. 16 more samples are taken from the pool of anchors having an IoU in the range $]0, 0.5]$ with respect to the ground truth. The remaining 16 samples are taken from the anchors which do not overlap with the ground truth bounding box. The classification loss is run over the 48 samples, which are balanced between positive, negative and hard examples. In contrast, the regression loss is only run over the 16 positive samples. Both losses are averaged across the total number of examples for the batch.

3D Tracking Regression Loss. We use the 48 anchors selected by the Region Proposal Network for the 3D tracking loss. Candidate shapes are defined by the points contained in the anchor boxes in 3D. The model shape is defined in training as the concatenation of all ground truth shapes along a tracklet. We learn to regress a cosine similarity between an encoded candidate shape $\Phi_{3D}(x)$ and the encoded model shape $\Phi_{3D}(\hat{x})$ to their Gaussian distance $\rho(d(\mathbf{x}, \hat{\mathbf{x}}))$ in the 3D search space. This tracking loss is shown in Equation (3).

$$\mathcal{L}_{tr} = \frac{1}{n} \sum_{\mathbf{x}} \left(\text{CosSim}(\phi_{3D}(\mathbf{x}), \phi_{3D}(\hat{\mathbf{x}})) - \rho(d(\mathbf{x}, \hat{\mathbf{x}})) \right)^2 \quad (3)$$

3D Completion Loss. Similar to Giancola *et al.* [9], we leverage a shape completion regularization in order to embed shape features within the Siamese latent space. The Chamfer Loss is used for this purpose between the model shape \hat{x} and its more complete reconstruction, \tilde{x} , as per Equation (4). The model shape is obtained as the concatenation of all ground truth shapes along a tracklet.

$$\mathcal{L}_{comp} = \sum_{\tilde{\mathbf{x}}_i \in \tilde{\mathbf{x}}} \min_{\tilde{\mathbf{x}}_j \in \tilde{\mathbf{x}}} \|\tilde{\mathbf{x}}_i - \tilde{\mathbf{x}}_j\|_2^2 + \sum_{\tilde{\mathbf{x}}_j \in \tilde{\mathbf{x}}} \min_{\tilde{\mathbf{x}}_i \in \tilde{\mathbf{x}}} \|\tilde{\mathbf{x}}_i - \tilde{\mathbf{x}}_j\|_2^2 \quad (4)$$

3.5. Training details

We train the region proposal network alongside the 3D Siamese network by minimizing the loss shown in Equation (5) using an image-centric sampling approach as is common with RPNs. In particular, we use $\lambda_{cls} = 1e^{-2}$, $\lambda_{reg} = 1$, $\lambda_{tr} = 1e^{-2}$ and $\lambda_{comp} = 1e^{-2}$.

$$\mathcal{L} = \lambda_{cls} \mathcal{L}_{cls} + \lambda_{reg} \mathcal{L}_{reg} + \lambda_{tr} \mathcal{L}_{tr} + \lambda_{comp} \mathcal{L}_{comp} \quad (5)$$

During training, we minimize the loss in Equation (5) using SGD with a momentum of 0.9. We start with a learning rate of 10^{-4} which we reduce by a factor of 10 after each plateau of the validation loss, with a patience of 2. Note that the training usually converges after a few epochs since our networks are pretrained.

3.6. Testing details

During inference, the pipeline is initialized with the ground truth bounding box for the tracked object in the first frame. Tracklets are processed in an online fashion looking only at the current and previous frames for each time step. The model PC is initialized to be the shape enclosed by the ground truth bounding box in the initial frame. For each tracking step, a search area is cropped around the previous location of the tracked object. BEV images are created for both the model PC and search PC to be processed by the RPN. The RPN generates C candidates which are then classified by the 3D Siamese network by comparing them with the model PC. Finally, the candidate with the best score from the 3D Siamese network is selected as the pose of the tracked object for the current frame.

4. Experiments

In this section, we show the superiority of our RPN module for generating proposals and compare it with the state-of-the-art proposed by Giancola *et al.* [9], who used Kalman

and Particle Filters as search methods. Successively, we show the results of the proposal selection method using the 3D Siamese network. Note that we initially focus on cars, but also report the results for cyclists and pedestrians.

Metrics. We report the One Pass Evaluation (OPE) [12] metrics from Single Object Tracking defined with the Success as the AUC of the IOU and the Precision as the AUC of the distance between both centers.

4.1. Proposals from BEV

Defining an efficient search space for 3D vehicle tracking is an arduous task. In effect, the sparsity of 3D point clouds impedes a 3D convolutional network from running over the whole search space without first sampling the point cloud. As a consequence, Giancola *et al.* [9] do not focus on the search portion of the problem and instead assume to have a very fine search space such that the ground truth box is always one of the candidates. However, this is not a realistic assumption to make as increasing the resolution of the search space in 3D incurs very high computational costs and thus having an exhaustive search space is impractical.

We compare our Region Proposal Network with other search methods such as Kalman (KF) and Particle Filtering (PF). The improvements from using an RPN over KF and PF are shown in Figure 3.

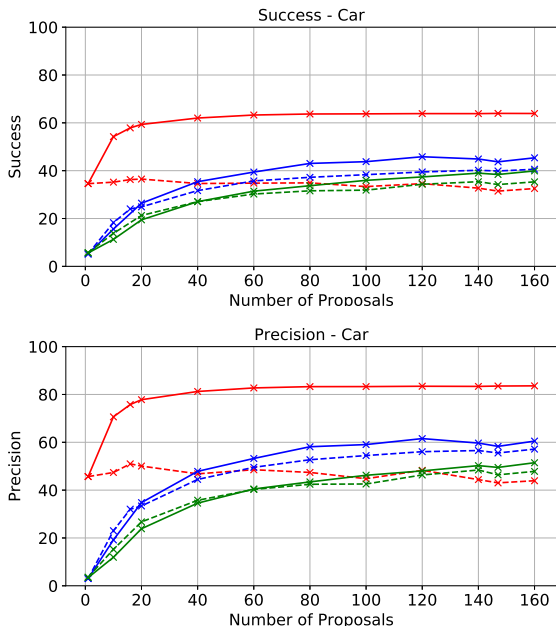


Figure 3. Proposal results for the Car class using RPN (red), Kalman Filtering (blue) and Particle Filtering (green). Continuous lines depict the upper bound results by picking the best proposal while dashed lines depict our 3D Siamese network discrimination.

In continuous lines, we show the tracking results of Kalman Filtering, Particle Filtering and Region Proposal

Network for a variable number of proposals/candidates when the best candidate among the proposals is chosen at each frame. In other words, these are the expected upper bounds when a perfect selection method over the candidates is assumed. The dashed lines represent the tracking results after our 3D Siamese network. As shown, the Region Proposal Network provides significantly better results than the Kalman Filtering and Particle Filtering candidates. We argue that the Region Proposal Network makes use of the visual features available from the BEV to propose meaningful candidates. In contrast, the other proposed methods are only relying on a probability distribution and hence are only able to learn motion priors.

It appears that RPN proposals saturate after 40 candidates while the Kalman and Particle Filters are not saturated yet even after 160 candidates. While Giancola *et al.* [9] leverage 147 candidates for their baseline, we only need around 10 candidates to beat their proposal methods for the same performances, which could provide a $15\times$ speed up for inference in the 3D Siamese similarity selection.

4.2. 3D Siamese Network Discriminator

The 3D Siamese network is used on top of the Region Proposal Network in order to discriminate the best candidate among the proposals. We plot in dashed lines in Figure 3 the tracking results when leveraging the similarity selection with the 3D Siamese tracker. The 3D Siamese network is able to select a good candidate from the list of proposals. Further results are shown in Table 1.

Table 1. OPE Success and Precision for different Search Space.

| Selection | 3D Siamese | Best candidate |
|---------------|------------------|------------------|
| KF (top-147) | 41.3 / 57.9 | 43.7 / 58.3 |
| PF (top-147) | 34.2 / 46.4 | 38.4 / 49.5 |
| RPN (top-1) | 34.6/45.7 | 34.6/45.7 |
| RPN (top-16) | 36.3/51.0 | 57.9/75.8 |
| RPN (top-147) | 29.1/40.9 | 26.3/36.0 |

The number of candidates selected from the BEV Siamese proposal module influences the final tracking results. Using too few candidates gives more confidence to the BEV Siamese proposals, with $topk = 1$ being the equivalent of relying exclusively on the BEV Siamese proposal network. On the contrary, using too many proposals in inference could confuse the latter 3D Siamese module, not able to pick the best one. As an example, using 147 proposals provides worse tracking performances than using only 16.

4.3. Point cloud aggregation

In this section, we are testing our inference architecture (Figure 2) using different model update methods. Since

point clouds are easy to combine by concatenating the points, we study what is the best way to create the model point cloud and BEV model in our pipeline. The model is created dynamically before each frame as a function of the previous results so far. In that setting, we are not using the future knowledge nor the ground truth but only the tracking results obtained so far. We test the effects of representing the model with only the previous result, only the first frame, a concatenation of the first and previous results, and as a concatenation of all previous tracking results.

As shown in Table 2, it appears that the more frames are used to generate the object model, the better the performances for tracking that object. Instinctively, we argue that storing more information about the 3D shape of an object obtained from different points of view enhances its capacity to be tracked. Note that the previous frame may drift apart and not follow the vehicle anymore after some bad results. Also, the first frame may only contain a few points that are not discriminative enough to describe a vehicle. However, leveraging a shape completion regularization enhances the semantic information of the 3D latent vector leveraged in the cosine similarity.

Table 2. OPE Success/Precision for different aggregation from the Point cloud and BEV models. Best representation aggregation shown in bold.

| Model | top-147 | top-16 | top-1 |
|-------------------------|--------------------|--------------------|--------------------|
| Prev. only | 29.5 / 38.6 | 35.0 / 47.6 | 27.3 / 37.9 |
| 1 st only | 29.9 / 38.3 | 35.7 / 48.4 | 27.3 / 37.9 |
| 1 st & prev. | 33.2 / 44.3 | 36.4 / 49.6 | 27.3 / 37.9 |
| All | 33.9 / 44.8 | 37.0 / 49.7 | 27.3 / 37.9 |

4.4. Generalization to more Objects

In this section we show the generalization capability of our network architecture to different classes of objects such as Cyclists and Pedestrians. Both classes are deformable by nature, however, in the KITTI dataset, they are considered to be enclosed within bounding boxes which do not vary in size with time. They can thus be analyzed with our framework without any modification.

Exhaustive Search. First, we present the tracking performances for Pedestrian and Cyclist with an exhaustive search as per [9]. Table 3 shows that training for shape completion in the ideal case of an exhaustive search improves the tracking performances for the Cyclist class. We believe that such objects can be considered as rigid in time. In particular, the motion of a the biker is negligible for the comprehensive shape. Table 4 shows the tracking performances for the Pedestrian class. In that case, Pedestrians may change significantly which impedes the construction of a reliable model shape representation. As a result, the completion loss has a negative effect for the final tracking performances.

Table 3. Ablation study for the Cyclist class using an exhaustive search space. Best results shown in bold.

| Cyclist | Success | Precision |
|---------------------------------|--------------|--------------|
| Ours – Completion only | 74.00 | 86.72 |
| Ours – Tracking only | 85.66 | 97.99 |
| Ours – $\lambda_{comp}@1e^{-6}$ | 86.91 | 99.81 |

Table 4. Ablation study for the Pedestrian class using an exhaustive search space. Best results shown in bold.

| Pedestrian | Success | Precision |
|---------------------------------|--------------|--------------|
| Ours – Completion only | 55.61 | 63.25 |
| Ours – Tracking only | 74.77 | 83.77 |
| Ours – $\lambda_{comp}@1e^{-6}$ | 71.38 | 80.43 |

Region Proposal Network. We highlight here the efficiency of the region proposal network for the additional classes. Figure 4 illustrates the proposal performance of Kalman Filtering, Particle Filtering and our Region Proposal Network, respectively on Cyclist and Pedestrian classes. The continuous lines show the results when picking the best candidate among the set of C proposals, while the selection made by the 3D Siamese network is presented with dashed lines. It appears that the proposal network outperforms the Kalman and Particle Filters in both cases, which means that the BEV representation provides enough information to generate meaningful candidates. Still, the selection from the Siamese BEV is confused between the top-20 proposals, but the 3D Siamese network is able to cope with the fine selection. Also, the BEV projection of the Pedestrian is smaller than for the Car and the Cyclist, which makes the BEV representation of Pedestrians less informative and more challenging than for Car and Cyclist.

3D Siamese Discriminator. Finally, we highlight that our 2D-3D Siamese network provides better tracking performances by leveraging less candidates than Kalman and Particle Filtering. Using only 20 candidates, our method achieves performances of 43.23/81.15 for Cyclists and 17.89/47.81 for Pedestrians. In comparison, Kalman Filtering reaches only 41.53/70.44 and 18.24/37.78 for the Cyclist and Pedestrian classes by leveraging 140 candidates. Not only do we improve tracking performances, but we improve them by leveraging less candidates, which implies time and complexity improvements as well.

5. Discussions

In this section, we provide further insights on our methodology for vehicle tracking.

2D vs 3D tracking. The 2D BEV provides greedy information to recognize the position of the vehicle in time. However, the BEV Proposal module is not able to identify a correct ranking over the other topk candidates. As a result, the

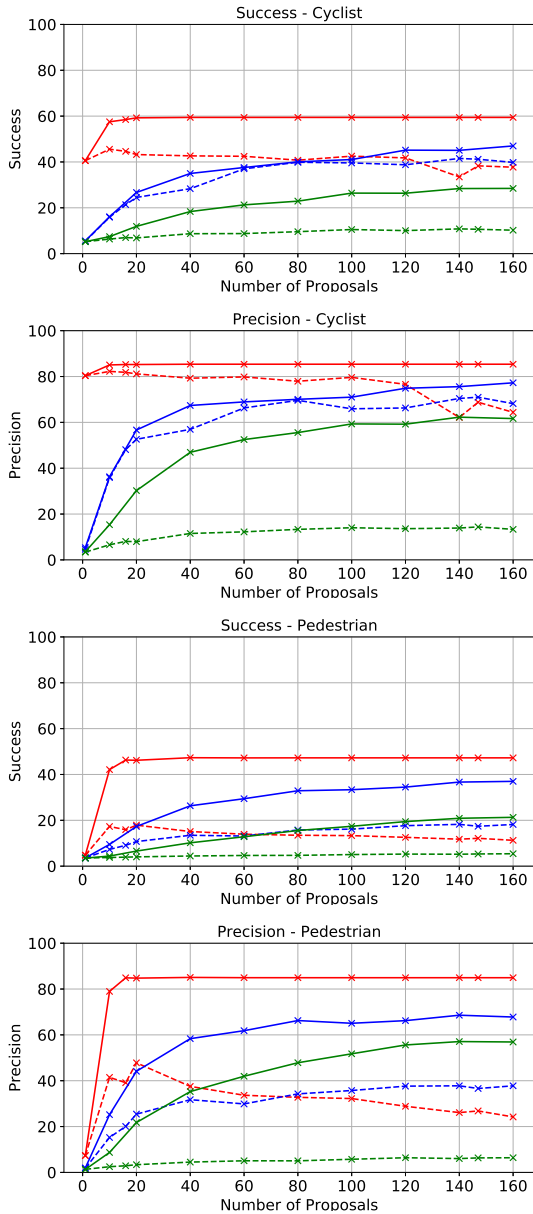


Figure 4. Proposals for Cyclist (top 2) and Pedestrian (bottom 2) classes using RPN proposals (red), Kalman Filtering (blue) and Particle Filtering (green). Continuous lines depict the upper bound results by picking the best proposal while the dashed lines depict our 3D Siamese network.

BEV Proposal module is not able to pick the optimal candidate. We believe this is due to the loss of information occurring in the BEV representation. As a result, leveraging the 3D Point cloud similarity selection with the 3D Siamese network improves drastically the tracking performances for all Car, Cyclist and Pedestrian.

Gap between proposals and tracking for RPN. The Region Proposal Network provides a huge improvement in

proposals generation with respect to Kalman and Particle Filtering. However, the 3D Siamese network is not able to cope with those candidates since there is a large gap in performance between the upper bounded results and those obtained with the 3D Siamese network. We believe this gap could be reduced by leveraging a variable variance for the Gaussian distance regression in the 3D Siamese network.

Extension to deformable objects. We show with the Pedestrian class that deformable objects do not improve with the shape completion loss. We argue that our model does not take into consideration the shape deformations that occur when a person is walking. However, leveraging a human body pose encoding could help understanding the complex Pedestrian shape. It would be possible to extend our methodology this way to include objects outside of the rigid body assumption.

Fast convergence. We noticed a fast convergence of our end-to-end training, with only a few epochs. We argue that both BEV proposal method and 3D point cloud tracking were pre-trained respectively on ImageNet and KITTI, and thus not much training is required to obtain a good model. Both networks fulfill two very distinct tasks that only slightly complete each other and thus joint training is not required.

Angle regression. We tried regressing the orientation of the bounding box as well but did not note any improvement. We argue that the anchors already provided a good enough resolution of 2.5 degrees without regression, and regressing a value under that resolution is not significant. Adding an angle regression only increases the method’s complexity and induces more errors during inference.

6. Conclusion

In this work, we emphasized the importance of searching for tracking. We leveraged the bijection between 2D BEV and 3D LIDAR bounding in vehicle tracking settings to efficiently generate proposals by searching in 2D. We used an RPN to generate proposals from LIDAR BEVs which are then discriminated using 3D point cloud information. We showed that RPNs are more efficient than Kalman and Particle Filters by a large margin. We then showed that using those proposals helps in selecting the optimal candidates with the 3D Siamese network for vehicle tracking. We did not only test that for Cars but also for the classes Cyclist and Pedestrian showing improvements in performances. This method could be extended in the future to perform fine tuning on the selected candidate box through the use of more detailed information contained in 3D point clouds. However, it is clear that a rough search on 2D BEVs could provide outstanding improvements on tracking performances.

References

- [1] V. Badrinarayanan, A. Kendall, and R. Cipolla. Segnet: A deep convolutional encoder-decoder architecture for image segmentation. *IEEE transactions on pattern analysis and machine intelligence*, 39(12):2481–2495, 2017. 1
- [2] L. Bertinetto, J. Valmadre, S. Golodetz, O. Miksik, and P. H. Torr. Staple: Complementary learners for real-time tracking. In *Proceedings of the IEEE Conference on Computer Vision and Pattern Recognition*, pages 1401–1409, 2016. 2
- [3] L. Bertinetto, J. Valmadre, J. F. Henriques, A. Vedaldi, and P. H. Torr. Fully-convolutional siamese networks for object tracking. In *ECCV*, pages 850–865. Springer, 2016. 2
- [4] A. Blake and M. Isard. The condensation algorithm-conditional density propagation and applications to visual tracking. In *Advances in Neural Information Processing Systems*, pages 361–367, 1997. 3
- [5] S. Chen. Kalman filter for robot vision: a survey. *IEEE Transactions on Industrial Electronics*, 59(11):4409–4420, 2012. 3
- [6] X. Chen, K. Kundu, Y. Zhu, A. G. Berneshawi, H. Ma, S. Fidler, and R. Urtasun. 3d object proposals for accurate object class detection. In *Advances in Neural Information Processing Systems*, pages 424–432, 2015. 3
- [7] X. Chen, H. Ma, J. Wan, B. Li, and T. Xia. Multi-view 3d object detection network for autonomous driving. In *Proceedings of the IEEE Conference on Computer Vision and Pattern Recognition*, pages 1907–1915, 2017. 2, 3
- [8] A. Geiger, P. Lenz, and R. Urtasun. Are we ready for autonomous driving? the kitti vision benchmark suite. In *Conference on Computer Vision and Pattern Recognition (CVPR)*, 2012. 2, 4
- [9] S. Giancola, J. Zarzar, and B. Ghanem. Leveraging shape completion for 3d siamese tracking. In *The IEEE Conference on Computer Vision and Pattern Recognition (CVPR)*, June 2019. 2, 3, 4, 5, 6, 7
- [10] K. He, X. Zhang, S. Ren, and J. Sun. Deep residual learning for image recognition. In *Proceedings of the IEEE conference on computer vision and pattern recognition*, pages 770–778, 2016. 1, 2
- [11] P. Karkus, D. Hsu, and W. S. Lee. Particle filter networks with application to visual localization. *arXiv preprint arXiv:1805.08975*, 2018. 3
- [12] M. Kristan, J. Matas, A. Leonardis, T. Vojir, R. Pflugfelder, G. Fernandez, G. Nebehay, F. Porikli, and L. Čehovin. A novel performance evaluation methodology for single-target trackers. *IEEE Transactions on Pattern Analysis and Machine Intelligence*, 38(11):2137–2155, Nov 2016. 2, 6
- [13] A. Krizhevsky, I. Sutskever, and G. E. Hinton. Imagenet classification with deep convolutional neural networks. In *Advances in neural information processing systems*, pages 1097–1105, 2012. 4
- [14] J. Ku, M. Mozifian, J. Lee, A. Harakeh, and S. L. Waslander. Joint 3d proposal generation and object detection from view aggregation. In *2018 IEEE/RSJ International Conference on Intelligent Robots and Systems (IROS)*, pages 1–8. IEEE, 2018. 2
- [15] B. Li, W. Wu, Q. Wang, F. Zhang, J. Xing, and J. Yan. Siamrpn++: Evolution of siamese visual tracking with very deep networks. *arXiv preprint arXiv:1812.11703*, 2018. 2
- [16] B. Li, J. Yan, W. Wu, Z. Zhu, and X. Hu. High performance visual tracking with siamese region proposal network. In *Proceedings of the IEEE Conference on Computer Vision and Pattern Recognition*, pages 8971–8980, 2018. 2, 4
- [17] B. Li, J. Yan, W. Wu, Z. Zhu, and X. Hu. High performance visual tracking with siamese region proposal network. In *The IEEE Conference on Computer Vision and Pattern Recognition (CVPR)*, 2018. 2
- [18] M. Luber, L. Spinello, and K. O. Arras. People tracking in rgb-d data with on-line boosted target models. In *Intelligent Robots and Systems (IROS), 2011 IEEE/RSJ International Conference on*, pages 3844–3849. IEEE, 2011. 2
- [19] W. Luo, B. Yang, and R. Urtasun. Fast and furious: Real time end-to-end 3d detection, tracking and motion forecasting with a single convolutional net. In *The IEEE Conference on Computer Vision and Pattern Recognition (CVPR)*, June 2018. 2, 4
- [20] M. Muller, A. Bibi, S. Giancola, S. Alsubaihi, and B. Ghanem. Trackingnet: A large-scale dataset and benchmark for object tracking in the wild. In *ECCV*, September 2018. 2
- [21] C. Musso, N. Oudjane, and F. Le Gland. Improving regularised particle filters. In *Sequential Monte Carlo methods in practice*, pages 247–271. Springer, 2001. 3
- [22] NuTonomy. The NuScenes dataset. <http://www.nuscenes.org>. Accessed: 2019-03. 2
- [23] C. R. Qi, H. Su, K. Mo, and L. J. Guibas. Pointnet: Deep learning on point sets for 3d classification and segmentation. *Proc. Computer Vision and Pattern Recognition (CVPR)*, IEEE, 1(2):4, 2017. 4
- [24] S. Ren, K. He, R. Girshick, and J. Sun. Faster r-cnn: Towards real-time object detection with region proposal networks. In *Advances in neural information processing systems*, pages 91–99, 2015. 1, 3, 4
- [25] B. Ristic, S. Arulampalam, and N. Gordon. *Beyond the Kalman filter: Particle filters for tracking applications*. Artech house, 2003. 3
- [26] S. Shin, I. Shim, J. Jung, Y. Bok, J.-H. Oh, and I. S. Kweon. Object proposal using 3d point cloud for drc-hubo+. In *Intelligent Robots and Systems (IROS), 2016 IEEE/RSJ International Conference on*, pages 590–597. IEEE, 2016. 3
- [27] S. Song and J. Xiao. Tracking revisited using rgb-d camera: Unified benchmark and baselines. In *Proceedings of the IEEE international conference on computer vision*, pages 233–240, 2013. 2
- [28] S. Song and J. Xiao. Deep sliding shapes for amodal 3d object detection in rgb-d images. In *Proceedings of the IEEE Conference on Computer Vision and Pattern Recognition*, pages 808–816, 2016. 3
- [29] J. Valmadre, L. Bertinetto, J. Henriques, A. Vedaldi, and P. H. Torr. End-to-end representation learning for correlation filter based tracking. In *Computer Vision and Pattern Recognition (CVPR), 2017 IEEE Conference on*, pages 5000–5008. IEEE, 2017. 2

- [30] C. Yang, R. Duraiswami, and L. Davis. Fast multiple object tracking via a hierarchical particle filter. In *Computer Vision, 2005. ICCV 2005. Tenth IEEE International Conference on*, volume 1, pages 212–219. IEEE, 2005. 3
- [31] T. Zhang, S. Liu, C. Xu, S. Yan, B. Ghanem, N. Ahuja, and M.-H. Yang. Structural sparse tracking. In *Proceedings of the IEEE conference on computer vision and pattern recognition*, pages 150–158, 2015. 3
- [32] T. Zhang, C. Xu, and M.-H. Yang. Multi-task correlation particle filter for robust object tracking. In *Proceedings of the IEEE Conference on Computer Vision and Pattern Recognition*, volume 1, page 3, 2017. 3
- [33] S. K. Zhou, R. Chellappa, and B. Moghaddam. Visual tracking and recognition using appearance-adaptive models in particle filters. *IEEE Transactions on Image Processing*, 13(11):1491–1506, 2004. 3
- [34] Y. Zhou and O. Tuzel. Voxelnet: End-to-end learning for point cloud based 3d object detection. *arXiv preprint arXiv:1711.06396*, 2017. 3
- [35] Z. Zhu, Q. Wang, L. Bo, W. Wu, J. Yan, and W. Hu. Distractor-aware siamese networks for visual object tracking. In *European Conference on Computer Vision*, 2018. 2